Glued-in CFRP and GFRP rods in block laminated timber subjected to monotonic and cyclic loading

Eleni Toumpanaki[1*] and Michael Ramage[2]

Abstract

Current advances in timber engineering with the use of timber at longer spans necessitate the use of high performance joints. Glued-in rods exhibit high axial load capacity and stiffness and are suitable for such applications. FRP rods can increase their durability and fire performance but ways to produce progressive failure mechanisms are necessary to enhance their resilience. In this study CFRP and GFRP rods glued-in block laminated timber with epoxy are investigated under both monotonic and cyclic loading. Joints with constant glue-line thickness and variable bond-line geometry are studied to induce progressive resin failure mechanisms. A stepped wedge shaped geometry with varying glue-line thickness and a mirrored version were investigated. The effect of elastic modulus (CFRP vs GFRP) and glue-line thickness on the bond strength, stiffness and material viscous damping are explored. CFRP rods exhibit 11% higher axial load capacity under monotonic loading but GFRP rods exhibit higher bond stiffness at the serviceability stage. The cyclic loading does not discount the bond performance and results in higher stiffness due to viscoelastic creep deformation. An increase in glue-line thickness results in higher axial withdrawal capacity and viscous material damping. Specimens with a wedge shaped bond-line exhibit superior mechanical performance. An FEA model is presented for a variable bond-line geometry and the numerical results agree well with the experimental findings.

Keywords: Glued-in rods, Bond strength, Fibre Reinforced Polymer (FRP), FE modelling.

[1] Lecturer, Department of Civil Engineering, University of Bristol, Queen's Building, University Walk, BS8 1TR, UK
*corresponding author: e-mail : eleni.toumpanaki@bristol.ac.uk

[2] Reader, Department of Architecture, University of Cambridge, 1-5 Scroope Terrace, CB2 1PX, UK

1 Introduction

Rods glued in timber have been used for timber connections at beam-to-column, column-to-foundation and truss joints, and also to provide member continuity (splice connections) and local strengthening of timber perpendicular to the grain [1, 2]. Despite the wider adoption of steel rods in such structural applications, there is no established design method in Eurocode 5 [3]. Various design formulas can be found in national guidelines (e.g. DIN [4] and New Zealand Guidelines [5]) relating the axial load capacity of glued-in rods to different key parameters (e.g. with or without the inclusion of a bond bar factor), and experimental results can often be contradictory. Moreover, there are no design guidelines for how stiff these connections should be, which is important to accurately predict the sway of a building. It is often up to the timber specialist to provide a holistic engineering solution including the design of these connections.

The use of composite materials such as carbon fibre reinforced polymer (CFRP) and glass fibre reinforced polymer (GFRP) rods can result in improved durability for these connections under high moisture content, lower weight and better chemical compatibility between the resin and the FRP rods [6]. FRPs are advantageous for structural applications near electromagnetic fields (e.g. MRI rooms) and can improve the fire performance of glued-in rods due to their lower thermal conductivity compared with steel [7]. Despite timber and epoxy acting as protective layers for steel rods against corrosion, paths of water ingress can form at the connection points due to differential deformations from shrinkage and creep effects or from splitting cracks due to temperature and humidity fluctuations during the design life of a structure. Moreover, visual inspection of glued-in rods is difficult after installation. Signs of steel corrosion even for zinc coated steel rods glued in glulam with either polyurethane or epoxy adhesive have been reported by Riberholt (1986) [8] after cyclic wetting/drying conditions with fresh and salt water. In the same study preloaded specimens were more vulnerable to corrosion attributed to cracks formed during loading. Current design guidelines (e.g. DIN 1052 [4]) limit the use of glued-in rods at service classes 1 and 2 and recommend the same modification factors as for glulam for the long-term bond performance of the glued-in rod joints regardless of the adhesive type.

Various structural adhesives have been investigated for glued-in rod connections over the years. The use of phenol-resorcinol (PRF) has resulted in decreased bond performance with increasing glue-line thickness attributed to higher shrinkage effects and the application of polyurethane (PUR) can yield bubbles at the wood/resin interface due to its reaction with the inherent timber moisture [9]. Epoxy (EPX) adhesives exhibit higher bond strength regardless of the glue-line thickness. Yet, different epoxies can yield different bond

performances and failure modes [10] and their standardisation is hindered due to constant advances in resin formulations that are usually proprietary to the manufacturers [11]. Feligioni et al. [12] showed that ductile epoxies in glued-in steel rods yield a more 'ductile' pull-out load – slip relationship and superior withdrawal resistance compared with brittle epoxies. However, the progressive curing of the ductile epoxy at ambient conditions resulted in more brittle failure modes and different trends were observed among the pull-out strength and the adhesive types and geometric parameters of the joint (e.g. the pull-out strength with the ductile epoxy was better correlated with the glue-line thickness). The importance of glue rheology/toughness has been highlighted by Serrano [9] with PRF glues exhibiting a distinct plateau at ultimate failure but lower shear strength when compared with epoxies. Ahmad et al. [13] studied the addition of microparticles such as liquid rubber (Albipox) and ceramic (Timberset) in structural adhesives for laminated veneer lumber (LVL) with the former yielding the highest critical strain energy release rate (GIC) and interlaminar shear and creep performance compared with the reference epoxy (CB10TSS). The addition of fillers is based on the assumption that particles can initiate cavitation and crack growth through local debonding and shear yielding improving the toughness of the epoxies [14]. Steel rods glued in LVL with epoxy reinforced with ceramic particles exhibited inferior axial load resistance compared with the standard epoxy, despite all failure modes lying within the wood regardless of the adhesive type [15]. Bio-adhesives for hardwood rods glued in softwood have also been investigated in [16] exhibiting comparable short-term mechanical performance to standard glues but much inferior durability performance in humid environments. The standardisation of structural adhesives should consider their long-term performance under environmental conditions (e.g. high humidity and temperature). Epoxies respond differently to the timber moisture content depending on their crosslinking molecular structure and their environmental degradation can be accelerated due to the presence of voids. However, the durability performance of glued-in rod connections relies on the mechanical response of the individual materials and their interaction under environmental conditions that affects the developed hygrothermal stresses. GFRP rods have lower transverse thermal coefficient (α_T=21-23 x 10^{-6}/ºC [17]) than CFRP rods (α_T=74-104 x 10^{-6}/ºC [17]) and tend to swell less than wood (α_T=23.56-31.06 x 10^{-6}/ºC [18]) under temperature fluctuations. Wood is more sensitive to dimensional changes due to moisture variations and is more responsive perpendicular to the grain. A thicker glue-line in FRP-wood composites can mitigate the hygrothermal stresses caused due to the differential shrinkage and swelling strains between the materials [19]. CFRP rods exhibit superior durability performance and lower susceptibility to creep rupture compared to GFRP and Aramid FRP rods [17]. Plevris and Triantafyllou [20] showed that CFRP and GFRP laminates were equally effective in restricting creep deflections

in reinforced wood members and AFRP laminates comparably led to higher curvatures and stresses. Mechano-sorptive creep tests of glulam beams reinforced with Basalt FRP rods under four-point bending showed that the reinforcement restrained effectively the shrinkage/swelling strains and had a negligible effect in the mechano-sorptive strain [21]. More research in the long-term effects of glued-in FRP rods and FRP reinforced timber beams is needed accounting for the creep response of the FRP reinforcement, timber and adhesive and the differential strain deformations. CFRP and GFRP rods are selected in this study due to their wider application in the construction industry and to account for their distinctive difference in stiffness in the bond performance of glued-in FRP rods.

Existing research on the use of FRPs for glued-in rod connections is limited to the use of GFRP rods due their lower cost (~ 1/3 of the CFRP cost) compared with CFRP rods. Madhoushi and Ansell [6] showed that GFRP rods glued in LVL with epoxy are more sensitive to the rate of loading at higher glue-line thicknesses (t=4 mm) with the majority of failures lying at the resin/rod interface. At smaller glue-line thicknesses (t=0.5 mm) the failure within the timber dominated. Zhu et al. [7] showed that the axial withdrawal capacity of GFRP rods glued in glulam with PUR adhesive (t=1.5mm) increases with increasing anchorage length and tends to plateau at slenderness ratios L_b/D>16. The dominating failure modes were wood/adhesive interfacial failure and wood plug failure with splitting taking place at larger rod diameters. The splitting failure modes can be the result of the decrease in the edge distances due to the consequent increase of the hole diameter with the use of a larger rod cross-section. CFRP and GFRP plates glued in glulam (GL24h) parallel to the grain with epoxy showed similar bond strength values for an anchorage length equal to the plate width in [22]. However, CFRPs exhibited consistently higher pull-out loads when glued perpendicular to the grain with a maximum increase up to 26% for a bonded length equivalent to three times the plate width. CFRP rods glued in glulam with epoxy failed by timber splitting in [23] despite the provision of adequate edge distances. The surface deformation profile with or without the addition of sand particles affected both the bond strength and stiffness. In all studies the glued-in FRP rods failed in a brittle manner when glued parallel to the grain but showed a plateau near the failure load when glued perpendicular to the grain. This can be attributed to a fibre stiffening/tying mechanism acting perpendicular to the grain during pulling out. Design models that clearly correlate the mechanical performance of the joints with the mechanical and geometric properties of the materials (adhesive, rod and timber) are necessary. The GIROD design equation [24] covers these principles but more experimental data is needed to verify its suitability in FRP rods. Moreover, there are no design equations for the axial stiffness of glued-in rods and the effect of cyclic loading that is important over the design life of a structure.

Fiber Reinforced Polymer (FRP) materials either in the form of sheets or rods are commonly adopted for shear and flexural reinforcement to strengthen both solid wood and glulam structural elements [25-30]. A lot of attention has been drawn in the structural rehabilitation of timber buildings due to the lower weight of the FRPs and ease of installation on site [31, 32]. The most commonly applied timber retrofit techniques are externally bonded FRP strips and near surface mounted (NSM) bars where the bond strength is dictated by the size and depth of the groove [33]. However, when FRPs are used as an internal reinforcement their fire performance is enhanced [26], the external wooden finish is aesthetically pleasing and the glue-line is protected against environmental conditions and impact loading. Considerable research has been conducted in the use of FRP reinforcement for timber structures and summaries of existing studies can be found in [26, 27]. It has been agreed among researchers that when FRPs are used as flexural reinforcement in timber beams, a significantly higher increase in flexural strength occurs compared to the flexural stiffness and there is an increase in ductile timber compressive failure modes due to kink band formation. Raftery and Whelan [28] showed that the use of compressive NSM GFRP rods in the top layer of the glulam beams increased the ultimate moment capacity but no signs of ductility were observed in the top compressive timber layer due to the adopted balanced reinforcement ratio. The use of circular grooves compared with square grooves enhanced the flexural performance of the single reinforced glulam beams and the quality of the wood in the bottom tensile layer could affect the failure modes and the development of timber compressive ductile failure. A higher energy absorption capacity and ductility was attained with pultruded GFRP channel sections externally bonded at the top and bottom faces of solid beech beams in [29] compared with single reinforcement arrangements and the use of L-shaped profiles. The greater sheathing of the beams with GFRPs resulted in a lower variance among specimens since local failures due to the presence of knots could be compensated by the stiffening contribution of the GFRPs. Micelli et al.[30] investigated the use of glued-in CFRP rods at both the compressive and tensile face in ‘spliced’ glulam beams. The ‘spliced’ glulam beams yielded similar flexural stiffness to the unreinforced beams at the serviceability stage but failed at lower loads. The CFRP-jointed beam with the longer anchorage length (L_b=1000 mm) exhibited the highest moment capacity and its performance was equivalent to the monolithic beam. Longitudinal splitting failure modes in the compression zone led to load drops and non-linear load-deflection response and wood plug failures in the glued-in rods in the tensile zone were followed up to ultimate failure. Blank [34]showed that high reinforcement ratios of FRP strips (ρ=0.0073 for GFRPs and ρ=0.0059 for CFRPs) result in ductile compressive failure modes in glulam beams under four-point bending and lower

reinforcement ratios lead to brittle failures modes such as tensile failure of the timber and reinforcement and timber/reinforcement interfacial failure. Blank and Frangi [35] developed an analytical model to predict the flexural capacity of FRP reinforced glulam beams accounting for the crack bridging effect of the reinforcement, the timber compressive softening response and the local hinge formation under bending. The model agreed well with experimental results and all the aforementioned failure modes were differentiated. The optimised use of FRP rods as flexural reinforcement in timber beams can lead to increased deformability and ductility via timber compressive softening enhancing the warning message before collapse. This is a challenge when glued-in FRP rods are used in timber elements subjected primarily to axial tensile forces (e.g. connections of diagonal members in a timber truss). Glued-in FRP rods fail predominantly in brittle manner due to a sudden wood/adhesive interface failure. An optimised design of the glued-in FRP rods can lead to progressive bond degradation, increased deformability and hinge rotation, and higher timber compressive softening response. The effect of cyclic loading on the bond strength and stiffness of the glued-in FRP rods and the resulting overall deformability and failure of the connected timber elements is also of interest.

Brittle failures with shearing off of a thin wood layer at the wood/adhesive interface have also been reported for steel rods [9, 12, 36]. Ductility with yielding of the steel rods can be provided at long anchorage lengths and with the provision of an unbonded length or a thinner rod cross-section near the loaded end where the axial stress is higher (e.g. GSA system [37]).To avoid brittle premature failure in either timber or glue, local strengthening of timber with screws running along the bonded length [38], plywood sleeves glued to the end grain [8] and wrapping of timber at the anchorage end [36, 39] have been studied. Another interesting method is the construction of epoxy ribs along the bonded length that act locally as wedge anchors increasing the total axial load resistance by engaging a greater wood surface area and enabling steel yielding [40]. Although this construction method seemed efficient with one resin rib and high grade steel rod (12.9), the use of multiple ribs led to brittle failure without steel yielding [41]. The use of thick resin ribs at small spacing accelerated the timber shear failure at the outer perimeter of the ribs. When FRP rods are glued in timber, the introduction of progressive bond failure is necessary to provide a non-linear load-deflection response close to failure. An efficient use of adhesive rib geometry along the bonded length can be beneficial towards a pseudo-ductile performance of FRP rods glued in timber by manipulating the shear stress concentrations to a tailored design axial load resistance as an alternative to bi-adhesive joints. An optimised glue-line geometry emphasising crack deviation, blocking and bridging can improve the toughness.

This study has three main research directions. Firstly, the effect of cyclic loading in the bond strength and stiffness of glued-in FRP rods is investigated to understand potential degradation effects. Viscous damping ratios are also reported to enable more accurate modelling of the joints. Secondly, the effect of the rod's elastic modulus in the bond performance of the glued-in rods is studied in relationship to the initial cost of the materials. CFRP and GFRP rods glued in timber are compared under both tensile monotonic and cyclic loading. Thirdly, ways to induce progressive bond degradation in glued-in FRP rods are investigated through geometric modification of the joint with different adhesive rib thicknesses along the bond-line. Experiments in glued-in FRP rods with constant glue-line thicknesses are carried out and used as a reference for the geometrically modified joints. These experiments enable to understand thoroughly the effect of the glue-line thickness in the performance of glued-in FRP rods. All key parameters are informative of progressive bond degradation. The adhesive adopted in this study is an epoxy reinforced with silica particles with an elastic modulus equivalent to the block laminated timber used. The adhesive is brittle to failure and thus emphasis is given to the introduction of mechanical pseudo-ductile performance.

2 Experimental Programme

2.1 Materials

This study uses pultruded FRP rods (Sireg, Italy) of different fibre type (glass versus carbon) with the same core rod diameter (D=10 mm), resin matrix (vinylester), fibre content (>65%), and surface deformation (helically wrapped and sand coated). The outer diameter of the rods (accounting for the external sand coating layer) is D_o=10.7 mm and D_o=11.1 mm for the CFRP and GFRP rods respectively according to ACI 440.3R-12 [42] guidelines. The bulging effect due to the helical wrapping is greater in GFRP rods. Figure 1 shows a typical GFRP and CFRP rod used in this study.

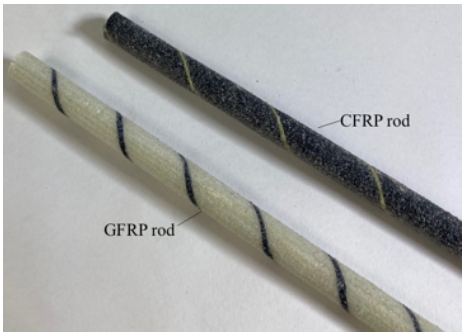

Figure 1: GFRP and CFRP rods with helical wrapping and sand coating layer.

The rods were glued in timber specimens using a two-component thixotropic adhesive of epoxy resin (Sikadur 30) containing silica particles (SiO_2) and special filler. The tensile mechanical properties and the mode II fracture toughness, K_{II}, of the adhesive were experimentally measured according to BS EN ISO 527 [43] and Ayatollahi et al. [44] respectively using a 2 kN Instron load cell capacity. Five Dumbell tensile specimens, 170 mm long and 5 mm thick, were preconditioned at 21.4 ± 1.5 °C and *RH*=50.9 ± 4.4 % and tested after 10 days under tension at 1 mm/min. Two strain gauges were used at the longitudinal and transverse direction to record the ultimate tensile failure strain and Poisson's ratio, since this data was not provided by the manufacturer. The experimental tensile Young's elastic modulus and ultimate failure strain were 23% higher and 5% lower than the nominal values. The moisture content of the specimens was 0.14% as calculated based on ASTM D6980-17 [45]. For the determination of the mode II fracture toughness, six specimens were preconditioned at 17.8 ± 1.6°C and *RH*=53.0 ± 5.0% and tested after 28 days under four-point bending at 1 mm/min. The moisture content of the fracture toughness test specimens was 0.41%. All mechanical properties are summarised in Table 1. The glass transition temperature of the epoxy adhesive, T_g, is 52°C as reported by the manufacturer and it is within the T_g range of commonly applied adhesives for glued-in rods. The timber laminations are expected to act as insulation and mitigate the effect of temperature fluctuations on the adhesive temperature. Finite element studies in glued-in steel rods by Faye et al. [46] demonstrated a 4-5 hrs delay between the ambient and adhesive temperature. The temperature of 50°C is defined as the upper limit for adhesives type II (EN 301 [47]) that are suitable for applications in service classes 1 and 2 [3].

The timber specimens derived from a block laminated spruce C24 [48] panel, made in Stora Enso's Ybbs (Austria) factory using their CLT process without the cross-laminated elements. The mechanical characterisation of the block laminated timber was carried out according to BS 373:1957 [49] and ASTM D143 [50] standards as shown in Table 1. The timber had an average moisture content of 9% according to BS 373:1957 [49] after being stored at 20.9 ± 0.6 °C and *RH*=51.0 ± 2.0 %.

Table 1. FRP rod and epoxy material properties.

	CFRP	GFRP	Epoxy glue
Longitudinal tensile elastic modulus - E_L (MPa)	130000[1]	46000[1]	13766 ± 1256[2,3] (5)
Average tensile strength, f_{ru} (MPa)	2450[1]	1000[1]	24.6 ± 4.8[2] (5)
Elongation at break, ε_{ru} (%)	1.8[1]	1.8[1]	0.2 ± 0.05[2] (5)
Poisson's ratio, v	N/A	N/A	0.25 ± 0.03[2] (5)
Average shear strength, f_{vu} (MPa)	N/A	N/A	16[1]
Stress intensity factor, K_{II} (MPamm$^{1/2}$)	N/A	N/A	77.3 ± 14.8[2] (6)
Mode II fracture toughness, G_{II} (MPamm)	N/A	N/A	0.43[4]
Glass transition temperature, T_g (°C)	>110[1]	>110[1]	52[1]

Timber density, $\rho_{,mean}$[2,5] (kg/m^3)	Compressive strength, $f_{c,0,m}$[2,5] (MPa)	Tensile strength, $f_{t,0,m}$[2,6] (MPa)	Elastic Modulus, $E_{0,m}$[2,6] (MPa)	Shear strength // to grain, $f_{v,//,m}$[2,5] (MPa)	Shear strength ⊥ to grain, $f_{v,\perp,m}$[2,6] (MPa)
430 ± 4.3 (5)	45.8 ± 2.3 (20)	72.6 ± 12.3 (7)	12670 ± 3204 (7)	6.4 ± 1.4 (10)	8.7 ± 1.6 (10)

Note 1: [1]Nominal values as provided by the manufacturer, [2] Experimentally measured values, [3] Elastic modulus determined as the secant modulus between 0.2-0.6F_u where F_u is the failure load, [4] $G_{II}=K_{II}^2/E_L$, [5] BS 373:1957 [49], [6] ASTM D143 [50],

Note 2: Average value ± Standard deviation (No of specimens)

2.2 Specimen Preparation

A 250 mm FRP rod was placed concentrically in a 70 x 70 x 55 mm timber block, parallel to the grain, and was glued with an epoxy layer of constant thickness (t=1, 3 and 5mm). The bonded length was 50 mm corresponding to 5D where D is the core diameter of the rod. Specimens with varying thickness over the bonded length were also prepared to understand the contribution of the mechanical interlocking effect on the bond strength and failure of glued-in rods. The basic geometric configuration adopted for both CFRP and GFRP rods is shown in Figure 2a. The smallest glue-line thickness of t=1 mm was adopted at the loaded end (LE: end closer to the crosshead of the Instron machine where the load is directly applied)) and the highest (t=3.0 mm) at the free end (FE). A bonded length of 10 mm was adopted for the 3.0 mm glue-line thickness to initiate a resin failure at the FE rather than a timber shear failure. This was judged suitable to maximise the pull-out load combined with a progressive debonding failure. This geometry is termed as 'wedge'(W). For ease of comparison, the mirrored geometry ('inverted wedge' - IW) was also tried with the highest glue-line thickness at the loaded end. This is representative of the counter-bore configuration in Broughton and Hutchinson [51]. The glue-line thicknesses adopted here are in accordance with previous studies in glued-in FRP [6] and steel

rods [12]. According to DIN [4] the maximum glue-line thickness should be specified by the manufacturer (product certificate) and no relevant data is available.

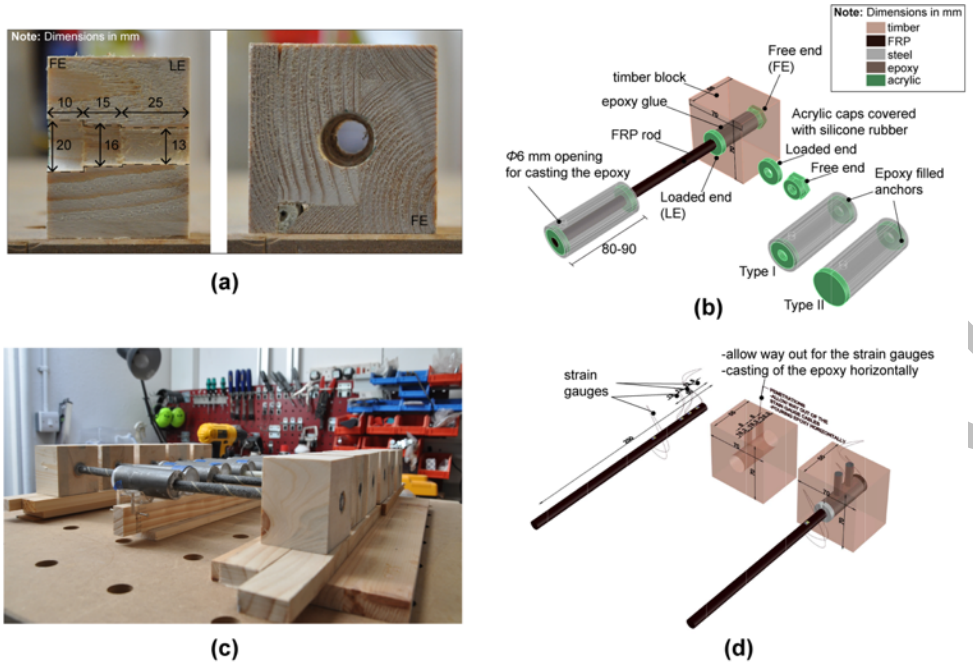

Figure 2: (a) Wedge geometry in glued in FRP rod specimens, (b) specimens with strain gauges along the bonded length, (c) 'pull-compression' test specimen and (d) alignment rig during epoxy curing.

To ensure the proper alignment of the FRP rod along the bonded length, acrylic caps were prepared and applied at both the loaded and free end (see Figure 2b). The caps were sprayed with a demoulding agent and covered with silicone rubber (Dow Corning) to enable their easy removal after curing of the epoxy glue. The epoxy was cast vertically in the holes and the specimens were left in that position for at least 1 day before the anchorage preparation. Sleeve anchors were used, to ensure a firm grip on the FRP rods considering their inferior mechanical performance in lateral compression. The anchors consisted of black mild steel tubes with an outer diameter D_o=31.75 mm, thickness, t=3.2 mm and length L=80-90 mm and were filled with epoxy (Sikadur 30 or Sikadur 33). The anchors were aligned horizontally based on the rig shown in Figure 2c. Two types of anchors (Type I and Type II) were used and Type I was preferred to accelerate the alignment procedure (see Figure 2c). The specimens are identified here as a-b-c, where 'a' denotes the fibre type (C: Carbon and G: Glass), 'b' denotes the glue-line thickness/geometry (1, 3, 5 mm, W and IW stand for the wedge and inverted wedge geometry) and 'c' denotes the type of loading (m: monotonic and c: cyclic).

To understand the bond stress transfer mechanism during pulling-out of the rod, one specimen from the C-5.0-m and G-5.0-m group was prepared with four strain gauges attached on the surface of the rod and equally

distributed over the bonded length (Figure 2d) . The strain gauge cables were guided through drilled holes of 8 mm diameter from one side of the specimen. To enable the attachment of the strain gauges, the sand coating layer of the FRP rods was removed with a blade along the bonded length for roughly a 5 mm wide surface area.

2.3 Test Method

To measure the bond strength of the FRP rods glued in timber blocks, the 'pull-compression' test method was selected due to its simplicity and ease of application for mechanical screening. The FRP rods were pulled out from the timber block that reacted against a fixed steel plate (see Figures 3a and 3b).

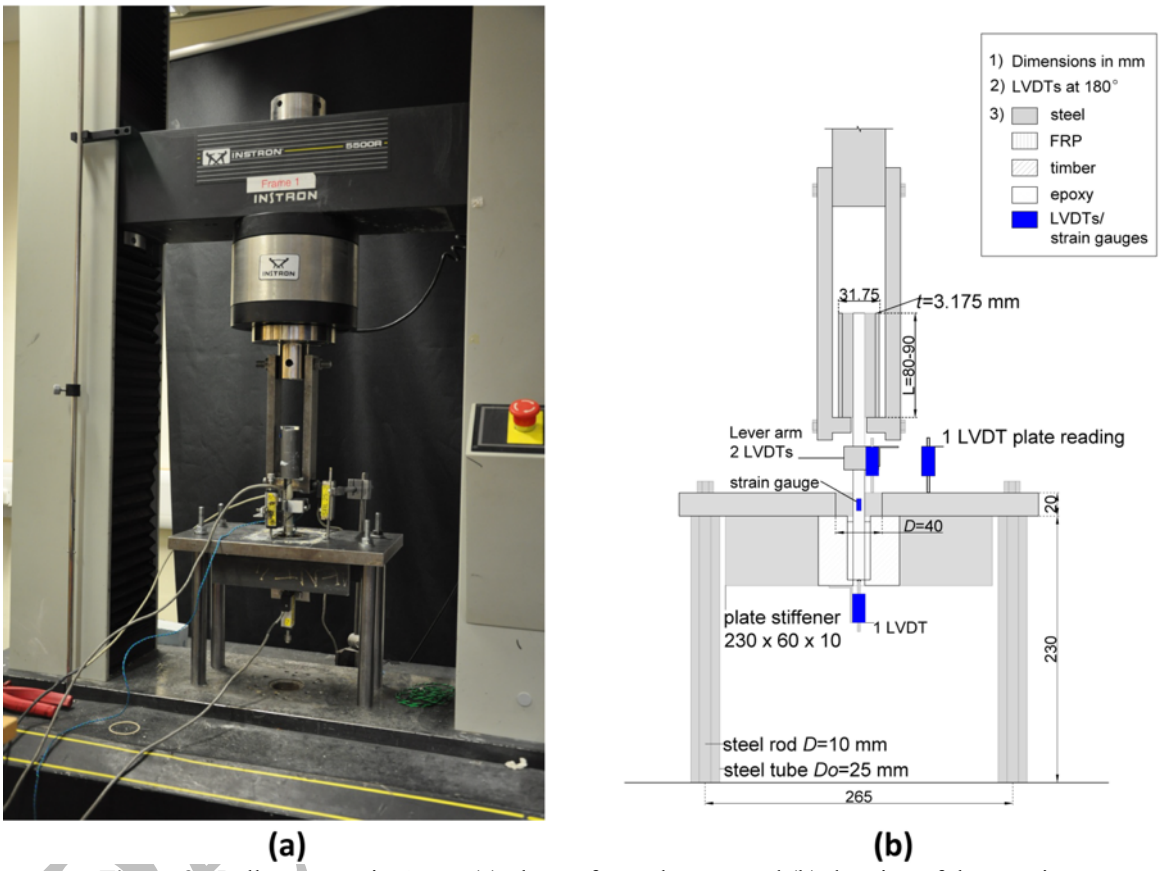

Figure 3: 'Pull-compression' test (a) photo of actual set up and (b) drawing of the test rig.

All specimens were tested after at least 10 days of curing of the epoxy glue. The tests were carried out in an Instron machine with a 150 kN load cell capacity in a displacement controlled mode. Five specimens from each of the 17 groups (85 samples in total) were tested under monotonic and cyclic loading at a displacement rate of 0.5 mm/min. The specimens with an inverted wedge geometry were tested only monotonically. The cycling regime consisted of three load-unload repetitions at three target loads of 0.20-0.25F_{us}, 0.4-0.5F_{us} and 0.60-0.75F_{us}, where F_{us} is the average pull-out failure load of each group tested monotonically, followed by loading up to failure. The experimental programme and the storage conditions of the specimens are summarised in Table

2. Slip values were recorded with two LVDTs (Linear Variable Differential Transformers) at the loaded end and one LVDT at the free end. Any displacement of the steel reaction plate was recorded with an LVDT during testing. Strain gauges were attached selectively at the loaded end of five GFRP and CFRP rods to experimentally measure their longitudinal elastic Young's modulus during the 'pull-compression' test method. The slip values at the loaded end were corrected for the rod extension and the plate displacement. The rod extension was calculated based on the experimental elastic Young's modulus values, that were 3% and 32% higher than the nominal values of the CFRP and GFRP rods respectively, and the free unbonded length of the rod between the two anchorage points (the sleeve anchor and the loaded end). The corrected slip values were considered to be more representative of a glued-in rod connection between two timber structural elements, where the unbonded length is negligible.

Table 2: Experimental programme

Group	Type of FRP rod	Glue-line thickness *t* (mm)	No of specimens	Loading regime	Storage conditions
C-1.5-m	CFRP	1.5	5	monotonic	21.5 ± 3.2°C (STDV) & 51.1 ± 7.8% (STDV)
C-1.5-c	CFRP	1.5	5	cyclic	
C-3.0-m	CFRP	3.0	5	monotonic	
C-3.0-c	CFRP	3.0	5	cyclic	
C-5.0-m	CFRP	5.0	5	monotonic	22.0 ± 2.3°C (STDV) & 53 ± 5.2% (STDV)
C-5.0-c	CFRP	5.0	5	cyclic	
C-W-m	CFRP	Varied (wedge)	5	monotonic	17.8 ± 1.6°C (STDV) & 53 ± 5.0% (STDV)
C-W-c	CFRP	Varied (wedge)	5	cyclic	
G-1.5-m	GFRP	1.5	5	monotonic	21.5 ± 3.2°C (STDV) & 51.1 ± 7.8% (STDV)
G-1.5-c	GFRP	1.5	5	cyclic	
G-3.0-m	GFRP	3.0	5	monotonic	
G-3.0-c	GFRP	3.0	5	cyclic	
G-5.0-m	GFRP	5.0	5	monotonic	22.0 ± 2.3°C (STDV) & 53 ± 5.2% (STDV)
G-5.0-c	GFRP	5.0	5	cyclic	
G-W-m	GFRP	Varied (wedge)	5	monotonic	17.8 ± 1.6°C (STDV) & 53 ± 5.0% (STDV)
G-W-c	GFRP	Varied (wedge)	5	cyclic	
G-IW-m	GFRP	Varied (inverted wedge)	5	monotonic	

2.4 Image Processing Technique

To relate the axial pull-out resistance of the glued-in rod specimens to the bond failure mechanisms and material mechanical properties, images of the failure modes at the LE and FE were taken with a Nikon D5300 and analysed using a Matlab script where each failure interface (e.g. wood failure or wood/adhesive failure) was interactively designated and the relevant shear strength value was assigned. The images were corrected for lens

distortion and a calibration factor according to a checkerboard was assigned at each failure interface. The shear strength properties were defined from Table 1 for a shear failure either within the epoxy or within the timber in radial or tangential direction. For shear failures at the wood/resin interface and resin/FRP interface, the average bond shear strength values were adopted as derived from the experimental pull-out loads of the relevant pure failure modes. The methodology was used for pure wood plug and mixed failure modes. In the specimens with a constant glue-line thickness the failure interface at the FE was assumed uniform along the bonded length (L=50mm). In the specimens with the varying thickness (IW, W) the failure interface at the LE was assumed constant over the 40 mm bonded length and the failure interface at the FE was considered for the remaining 10 mm bonded length where different failure modes were observed between the ends. The theoretical pull-out loads were compared with the experimental ones and enabled a better understanding of the failure mechanism in the glued-in rod specimens.

3 Results and Discussion

3.1 Axial withdrawal capacity

Figure 4a shows the average pull-out load values, F_u, for each glue-line thickness and geometry (t=1.5, 3.0 and 5.0 and 'wedge' and 'inverted wedge') and each rod material (CFRP and GFRP) after monotonic and cyclic loading. Figure 4b shows the average bond strength values as derived from the pull-out failure loads normalised by the surface area of the timber hole diameter, assuming a uniform bond stress distribution over the bonded length. The hole surface area was adopted as a reference area since the majority of bond failure modes occurred in the wood/resin interface. For the 'wedge' and 'inverted wedge' geometry an average diameter of D=15.5 mm is considered as derived from the hole surface area and the bonded length at each glue-line thickness. The error bars indicate one standard deviation. The red dots represent the specimens with the 4 strain gauges over the bonded length that were tested monotonically. These specimens were excluded from the group's average values, because the occupied volume of the cables of the strain gauges resulted in an increased number of voids, as visually inspected after testing, and discounted bond performance. The specimens with a constant glue-line thickness t=1 and 2 mm and 3 mm had a timber moisture content of 9.7 ± 0.6 % (STDV) and 8.7 ± 0.5 % (STDV) respectively as measured with a moisture meter (EXTECH M0220) after testing. The specimens with the modified geometry were dry and their moisture content was 8.1 ± 0.7 % (STDV).

All rods (CFRP and GFRP) showed an increasing trend in the average pull-out load with a rise in the glue-line thickness as a result of the increasing surface area. Rises up to 43 and 53% were recorded under static loading

with a 3.5 mm increase in the glue-line thickness for CFRP and GFRP rods respectively. Under cyclic loading the differences were 32% and 88% for the CFRP and GFRP rods respectively. An increase in timber moisture content up to 1% between several groups (e.g. C-1.5-m and C-3.0-m compared with C-5.0-m) is expected to result in a timber shear strength reduction of 2.5% [52]. A proportionally similar decrease in the pull-out load can be assumed. This is more relevant to specimens that failed in timber. The moisture content variations between groups are expected to play a negligible difference between the groups given the much higher differences observed due to the glue-line thickness. Different trends were observed in terms of normalised load and bond strength values, as shown in Figure 4b. CFRP rods showed a 7% decrease in the bond strength by comparing the C-1.5-m with the C-5.0-m group and GFRP rods showed a negligible difference for the same glue-line thickness variations. Variations, up to 22%, in the bond strength (G-5.0-c vs G-1.5-c) are more pronounced under cyclic loading due to the inherent differences in pull-out load. The axial pull out resistance of the 'wedge' specimens is comparable to that of the specimens with the thickest glue-line thickness (t=5.00 mm) irrespective of the type of FRP rod. The 'inverted wedge' specimens (G-IW-s) yield pull-out loads in the range of the average values of the G-3.0-m and G-5.0-m.

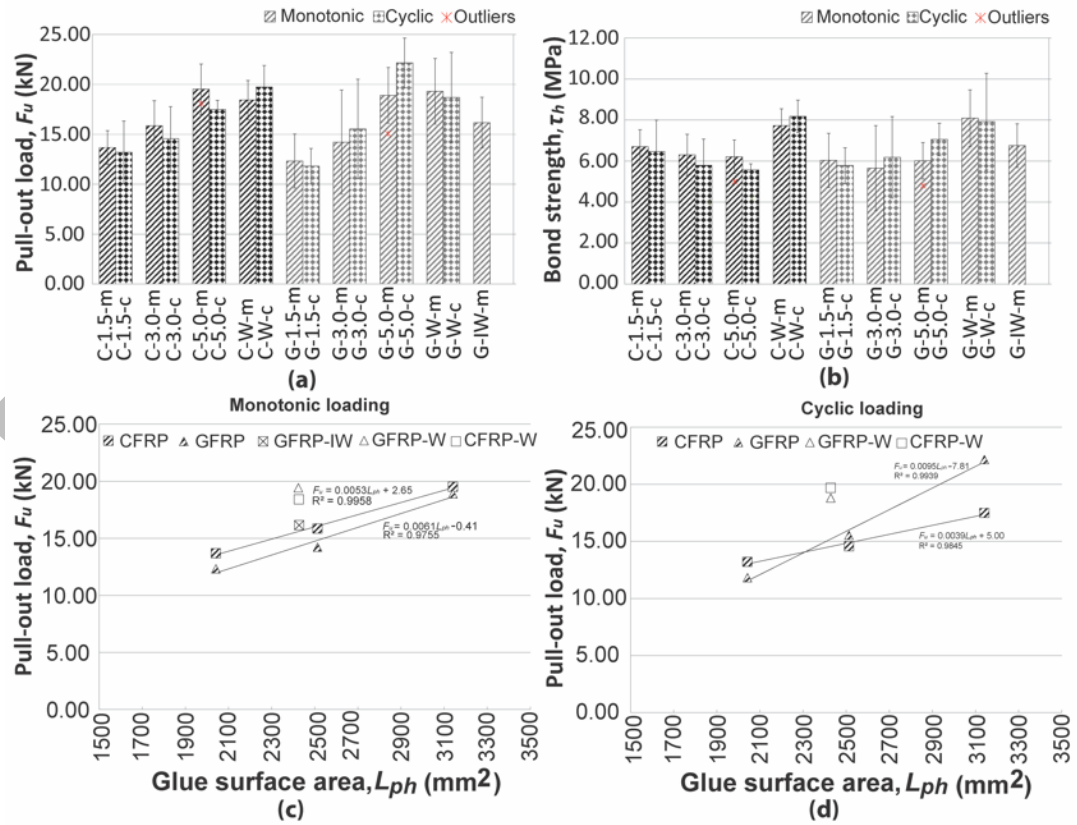

Figure 4: (a) Pull-out failure load, (b) Bond strength, (c) Monotonic pull-out load versus glue surface area and (d) Cyclic pull-out load versus glue surface area.

CFRP rods exhibited consistently higher average pull-out loads than the GFRP rods under monotonic loading irrespective of the glue-line thickness. The only exception lies in the wedge configuration. The difference between the two materials was more dominant at smaller glue-line thicknesses (t=1.5, 3.0 mm) where CFRP rods showed 11% higher axial load resistance. For a given strain amplitude, higher shear stress concentrations are expected for glued-in CFRP rods due to their higher elastic Young's modulus. This can result in shear failures within the resin leading to higher axial withdrawal resistance due the higher glue shear strength. As will be discussed in section 3.4, most resin failures were experimentally observed in glued-in CFRP rods. This can also be attributed to the lower mechanical interlocking effect between the CFRP rods and resin due to their shallower indentations (lower apparent outer diameter D_o compared with GFRP rods). The cyclic loading seems not to greatly affect the average axial withdrawal resistance of CFRP rods given the observed standard deviation among specimens and the inherent material variability. A maximum 10% decrease is recorded for a glue-line thickness t=5.0 mm (C-5.0-c versus C-5.0-m) after cyclic loading. It should be noted that one of the five specimens in group C-1.5-c failed at the first loading of the 3rd cycle ($0.66F_{us}$) at 8.09 kN. Under cyclic loading GFRP rods seemed to perform better and yielded the maximum average axial load resistance among the groups, F_u=22.16 kN, for a glue-line thickness t=5.0 mm. This can be the result of residual stress relief and redistribution (e.g. from shrinkage effects during curing and environmental conditions) combined with the higher compliance of GFRP rods. The experimental findings of the G-1.5-m group (F_u=12.32 kN) agree well with Mettem et al. [15] where an average pull-out load of F_u=12.2 kN was recorded for GFRP rods (D=8.0 mm) glued into LVL with a 2 mm epoxy glue-line thickness and a 60 mm bonded length and tested with the 'pull-compression' method. The experimental results suggest that the increase in the pull-out load and the hole surface area are linearly related for both types of rods (see Figure 4c &d) but an approximately six times increase in the glue volume can lead to a rise in axial load resistance of up to 88% (G-5.0-c versus G-1.5-c). Deviations from the linear relationship between the axial withdrawal resistance and the hole surface area are observed for the wedge-shaped specimens where a much higher load can be achieved with a more optimised use of glue material. A 50% average increase in bond strength can be derived with a twofold increase in glue volume and a wedge shaped geometry. Therefore, the relevant benefits in the axial withdrawal resistance from an increase in the glue volume and consequently cost should be estimated using engineering judgement. Long-term swelling and shrinkage effects due to temperature and humidity variations in the environments should be considered in relationship to the glue-line thickness. Lower transverse stresses at the wood interface have been reported in [53] with increasing glue-line thickness.

3.2 Bond stress-slip plots

The bond stress-slip plots for the CFRP rods under cyclic loading are depicted in Figure 5 for the different glue-line thicknesses studied. The slip values refer to the loaded end. It can be observed that there is no decrease in the gradient and thus the stiffness of the glued-in rod connections upon cyclic loading. An increase in the residual slip values after unloading is detected and it is more pronounced with increasing loading and glue-line thickness. This is attributed to cyclic creep that is representative of viscoelastic materials such as timber and epoxy resins. The failure of the CFRP rods glued in timber parallel to the grain was mostly brittle with a sudden drop in bond strength up to 94% of the peak values irrespective of the glue-line thickness. GFRP rods exhibited similar performance. Specimens with the 'wedge' geometry show limited signs of progressive failure at ultimate failure load. A load plateau at failure or stiffness degradation near the failure load were not discernible. A post-failure residual strength could be observed in a few specimens (Figure 5d) but similar bond stress-slip plots could be detected in a few specimens with a constant glue-line thickness particularly in mixed failure modes. A relationship between the geometry of the joint, progressive bond failure mechanisms and bond stress-slip plots could not be defined for the G-IW-m group that showed similar behaviour with the rest of the specimens. More experimental data is statistically needed to derive firm conclusions. The lack of a pseudo-ductile performance is attributed to the short bonded length adopted in this study and more experimental data is needed at longer anchorage lengths. At high anchorage lengths the non-uniform bond stress distribution is more pronounced and the shear stress concentrations at the free end are lower [40].

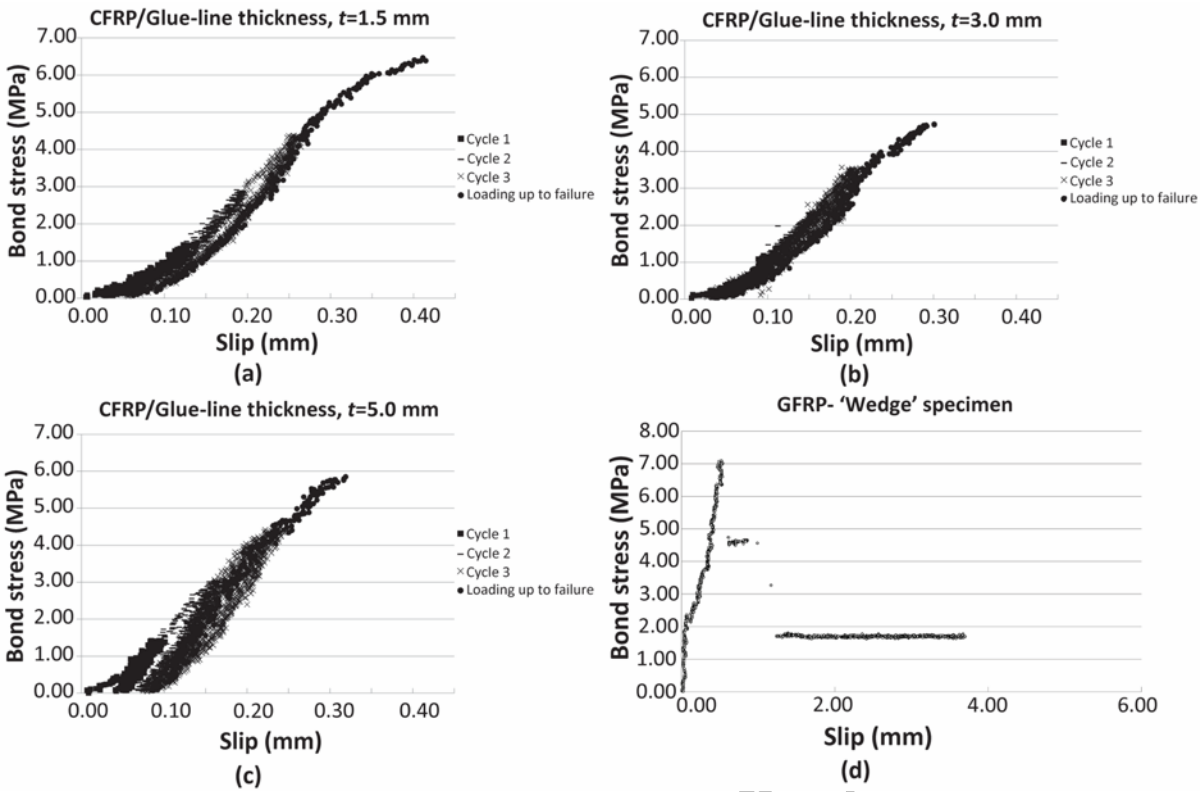

Figure 5. Bond stress-slip plots at cyclic loading for a CFRP rod with (a) glue-line thickness, t=1.5 mm, (b) glue-line thickness, t=3.0 mm, (c) glue-line thickness, t=5.0 mm and (d) at monotic loading for a GFRP-W specimen.

3.3 Secant stiffness

Figures 6a and 6b depict the secant stiffness derived from the pull-out load versus slip plots at the ultimate limit state (ULS) and serviceability limit state (SLS). The serviceability limit state was defined between 10 and 40% of the ultimate failure load, F_u, where structures are mostly expected to be loaded during their design life and to align with the slip modulus definition, K_{ser}, for steel dowel connections. For the specimens tested up to failure after cyclic loading the secant stiffness definition was corrected for any residual slip at zero load. The stiffness at ULS was defined between 10 and 100% of F_u. The average values of at least four specimens are considered.

The secant stiffness at both ULS and SLS exhibited high values for a glue-line thickness of t=5.0 mm under both monotonic and cyclic loading. Most specimens had a higher secant stiffness after cyclic loading with maximum values of K_{SLS}= 115.3 kN/mm, K_{SLS}=219.7 kN/mm and K_{ULS}=104.7 kN/mm and K_{ULS}= 119.7 kN/mm for the groups C-5.0-c and G-5.0-c respectively. This was attributed to the stiffer response observed with increasing loading combined with the corrected slip values for the residual deformation. The difference in the

stiffness between glue-line thicknesses t=1.5 and 3.0 were limited to around +/- 20% under cyclic loading. Under monotonic loading the stiffness of the glued-in rods for a glue-line thickness of t=3.0 mm shows the lowest secant stiffness at both SLS and ULS irrespective of the type of FRP rod. This might be related to residual internal stresses during curing combined with storage humidity conditions (swelling and shrinkage) that are more dominant with increasing glue-line thickness though not inferred in thicker glue-lines. At constant glue-line thicknesses the stiffness at ULS was similar irrespective of the type of fibre but GFRP rods showed higher stiffness up to 90% at SLS. The wedge-shaped specimens exhibited similar stiffness at ULS irrespective of the type of fibre and average values of K_{ULS} =34.4 kN/mm under monotonic loading and K_{ULS} =77.3 kN/mm under cyclic loading were recorded. Their stiffness values under monotonic loading for both ULS and SLS was equivalent to the specimens with a glue-line thickness, t=3.0 mm, apart from the stiffness, K_{SLS} for groups G-W-m and G-3.0-m. Yet, the wedge-shaped geometry showed up to 2.6 times higher stiffness than the group with a glue-line thickness, t=3.0 mm, under cyclic loading. The G-IW-m specimens had twice the stiffness of G-W-m and this is attributed to the position of the counter-bore (thickest glue-line) at the loaded end. The stiffness values of the specimens with the attached strain gauges are also indicated in Figure 6 with a star symbol for ease of comparison. These specimens exhibited substantially lower stiffness attributed to the occupied volume of the cables resulting in increased void content. For ease of comparison the slip modulus of a single dowel connection with a 10 mm steel dowel for the same timber grade is 3.7 kN/mm per shear plane according to Eurocode 5 and can vary up to 14.8 kN/mm accounting for two shear planes and a steel-to-timber connection. However, a higher stiffness up to 38.4 kN/mm has been experimentally reported by Reynolds et al. [54] for a single dowel connection with a 12 mm steel dowel in C16 Sitka spruce.

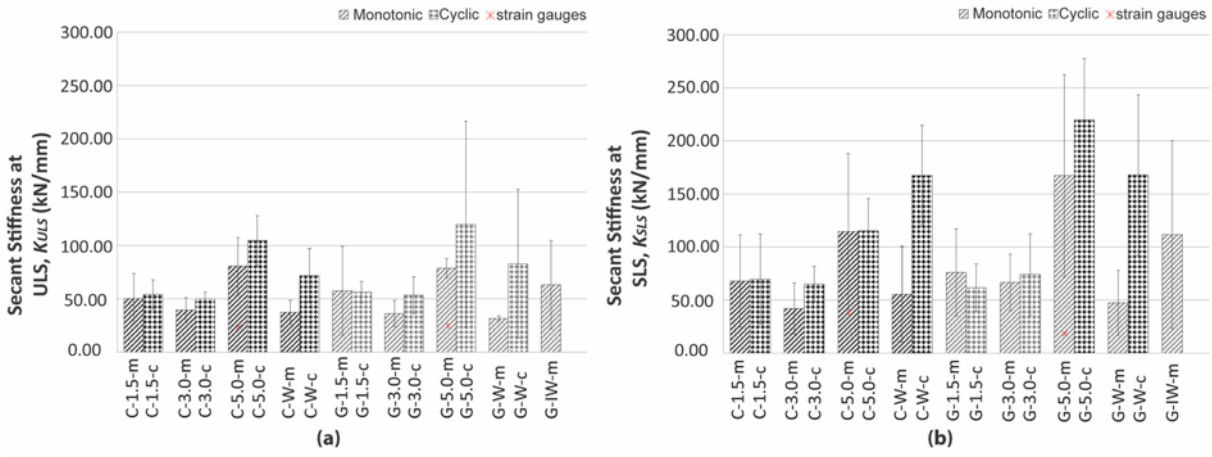

Figure 6: (a) Secant stiffness at ULS and (b) Secant stiffness at SLS.

3.4 Bond failure mechanisms

The majority of the specimens (62 out of the 85 tested in total) failed at the wood/resin interface (W/R) (see Figure 7d) occasionally followed by a wood plug failure (WP) or resin/FRP failure (R/F). The definition of the bond failure mechanisms adopted in this study is depicted in Figure 7c. In the resin/FRP failure mode the failed interface was mostly between the external sand coating layer and the core rod indicating a good adhesion between the external epoxy layer and the FRP and lower shear strength in the FRP rod between the small indentations. In Figures 7a and 7b the failure mechanisms with respect to the glue-line thickness/geometry and the experimental pull-out load are classified for the clear and mixed-mode bond failures. The highest axial load resistance is observed for resin/FRP interface failure modes at a constant glue-line thickness of t=5.0 mm and in the wedge shaped specimens. The majority of the resin/FRP interface failures were associated with CFRP rods attributed to the higher axial stress concentrations developed at this interface as a result of their higher axial stiffness. This is also the outcome of a less pronounced mechanical interlocking effect as discussed in section 3.1. Considerable variations in the pull-out load lie among clear failure modes, such as wood plug and wood/resin interface, and a direct relationship between the bond strength of the glued-in rods and the failure modes cannot be derived. This is investigated in more detail in section 3.5 with an image processing technique. Splitting failures are not linked with lower failure loads, but the effect of the reaction plate in the adopted test method ('pull-compression') should also be considered. The compression stresses acting on the loaded timber face from the reaction plate might negate any propagation or widening of the initial splitting cracks and thus leading to an erroneous increase in axial load resistance.

In 18 specimens out of the 85 tested in total, the wood plug failure extended up to the hole of the reaction plate. This was mostly observed in the groups C-1.5-m and C-1.5-c. This indicates that the 'pull-compression' test method can affect the bond failure and possibly the experimental axial withdrawal resistance compared with the 'pull-pull' test method. In the wood plug failure the failed surface mostly propagated along the growth rings at the latewood/earlywood interface or within the earlywood, as schematically shown in Figure 7c(i). This is attributed to the interfacial shear stresses between earlywood and latewood due to the inherent differences in density and thus stiffness. However, the crack propagation could also be initiated transversely to the growth rings at the vicinity of the wood/resin interface forming a wood plug failure (Figure 7e (ii)). In some specimens the wood plug failure was limited to one lamina of the timber block (Figure 6e (ii)) and the crack pattern did not extend to the adjacent one. Therefore, the wood plug failure mechanism and the relevant bond strength values are related to the timber density (as suggested by Steiger et al. [37]), compared with the wood/resin and

resin/FRP failure mechanism. Variations in the bond strength due to material variations are also expected. By observing the wood plug failure pattern, the peak failure load seems to depend on the wood shear strength in both the longitudinal/radial and longitudinal/tangential plane.

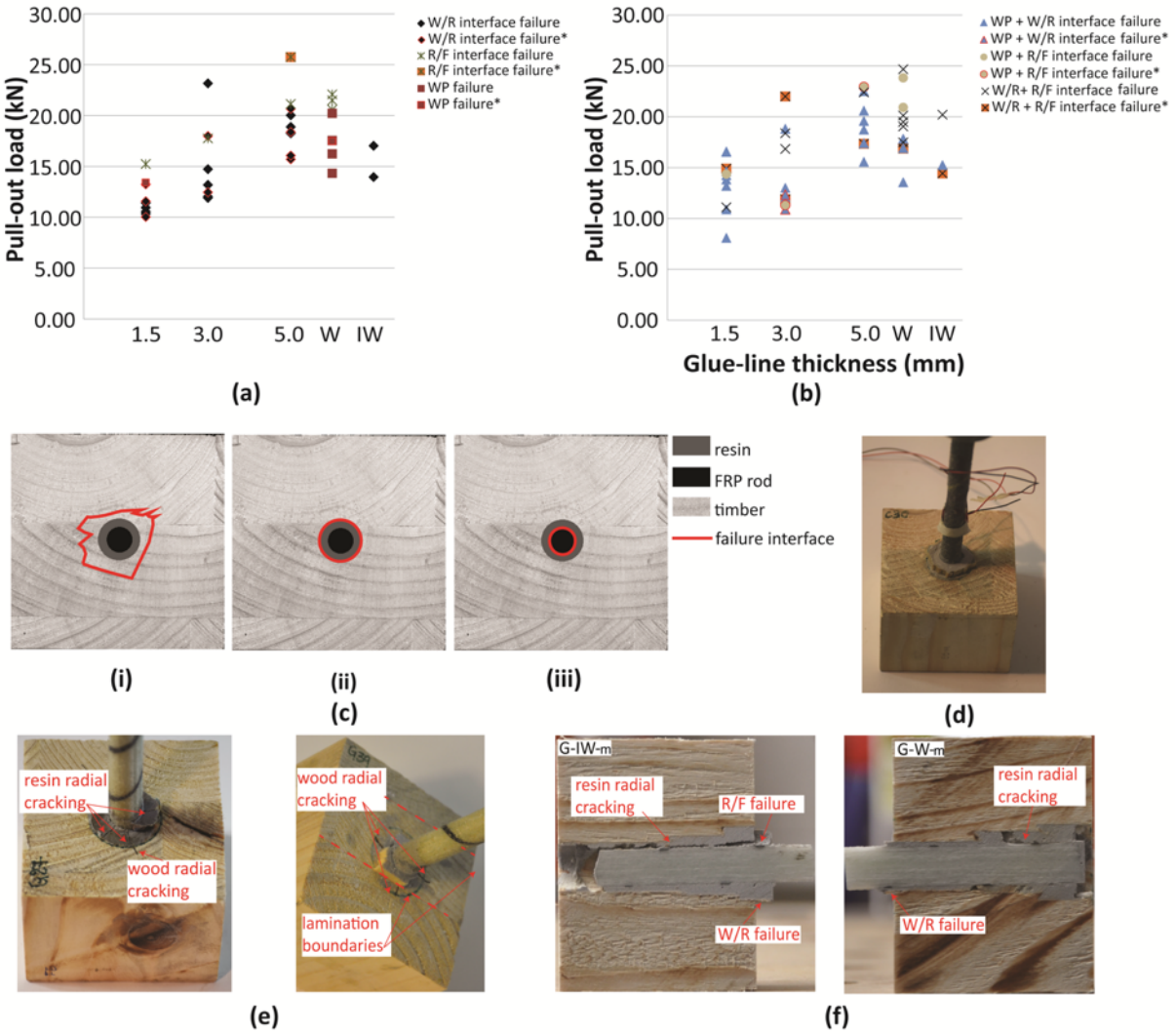

Figure 7: Pull out load versus glue-line thickness (a) clear bond failure modes and (b) mixed bond failure modes, (c) definition of bond failure modes (i) wood plug failure, (ii) wood/resin interface failure and (iii) resin/FRP failure, (d) actual photo of a typical wood/resin interface failure, (e) wood and resin radial cracking at failure and (f) typical crack path for the G-IW-m and G-W-m group.

Noise of imminent failure followed by occasional visually detected radial cracks were observed during the cyclic loading at $0.75F_{us}$. The radial cracks formed either within the resin layer at the highest glue-line thickness, t=5.0mm, or extended within timber at low glue-line thicknesses, t=1.0 and 3.0 mm (Figure 7e). In the latter case resin cracks were also observed at the free end of the specimen. The radial cracking indicates that the bond of CFRP and GFRP sand coated tendons glued-in timber acts at an angle resulting in the development of hoop stresses, as derived from a thick-walled analysis, exceeding the material's tensile capacity (either resin

or timber). Experimental results for sand coated GFRP bars embedded in a concrete ring have shown that bond develops at an angle of α=30° [55].

Splitting was associated with 18 bond failure mechanisms and it was mostly observed in specimens with a thicker glue-line (t=3.0 and t=5.0 mm). Splitting cracks propagated along the growth rings, were restricted in some cases within the lamina and they usually developed in the vicinity of a knot as observed in the face/edge grain of the specimen. More splitting failures were observed in GFRP rods at a glue-line thickness of t=1.5 mm and t=3.0 mm and for CFRP rods this was dominant at a glue-line thickness of t=5.0 mm. This indicates that the recommended minimum edge distances of 2.5D [4] or 3.5D for pull-pull test methods [56] are not suitable for FRP rods glued-in timber. Splitting cracks at much greater edge distances, 6.4D, have been reported in De Lorenzis et al. [23] for CFRP bars glued-in glulam timber (timber grade equivalent to C50) and tested with the 'pull-compression' method. A higher number of splitting bond failure modes have also been recorded for Near Surface Mounted GFRP ribbed rods used in normal strength concrete when a smaller groove size was applied [57]. Similar CFRP ribbed rods but with less pronounced ribs exhibited failure at the epoxy-concrete interface. A greater splitting tendency has also been observed by Achillides & Pilakoutas [58] in GFRP bars used as a reinforcement in concrete beams and when an adequate concrete cover was not provided. This was attributed to the lower Elastic modulus of the GFRP bars that affects their deformability both in the longitudinal and transverse direction (Poisson's ratio effect). Nevertheless, the rod's contraction from the Poisson's ratio effect should result in compressive stresses in the hoop direction negating the development of splitting and radial cracking. De Lorenzis et al. [23] showed that the splitting bond strength depends on the depth of the provided cover when FRP rods are glued in timber parallel to the grain by adopting a thick walled analysis. However, this analytical approach is valid for isotropic materials and might not be suitable for anisotropic materials like timber. Madhoushi & Ansell [59] showed that the increase in glue-line thickness for GFRP rods glued-in LVL alleviates the axial stress concentrations across the glue-line using Finite Element analysis.

All the wedge-shaped specimens exhibited a resin/FRP interface failure at the free end regardless of the type of FRP rod (Figure 7f). This suggests that cracking propagates towards the weakest resin/FRP interface. The presence of microvoids between the sand coating and resin layer due the dense distribution of sand particles (as also observed elsewhere [60]) can enable this crack path development. The inverted wedge specimens usually exhibited a wood/resin interface failure that extended to a wood plug failure at the free end. Mixed modes combined with resin/FRP interface failure up to the free end were also observed (Figure 7f).

3.5 Image Processing technique

Figure 8a shows the theoretical pull-out load, F_{theor1}, as derived based on the bond strength of the W/R and R/F interfaces and the timber shear strength perpendicular and parallel to the growth rings with respect to the experimental values, F_{exp}. Clear and mixed modes of wood plug failure are considered. The theoretical values are consistently greater than the experimental ones by assuming that the total shear failure plane is related to the axial load resistance of the glued-in rods. Figure 8b shows the theoretical pull-out load, F_{theor2}, without considering the timber shear failure planes at a greater distance from the wood/resin interface. These are usually the failure planes that develop transversely to the growth rings (Figure 8d). A better correlation between the theoretical and experimental axial load resistance can be observed. Videos were taken in selected specimens with a microscope at the loaded end during the 'pull-compression' tests. These videos suggest that in wood plug failure modes the initial drop in the pull-out load-displacement plot correlates with the shear failure planes developed adjacent to the wood/resin interface. The residual axial load resistance before the second final drop in the pull-out load versus displacement plot is related to the timber failure planes closer to the plate hole of the test rig. The relationship between the theoretical , F_{theor_res}, and experimental, F_{exp_res}, residual pull-out loads is depicted in Figure 8c, where $F_{theor\_res} = F_{theor1} - F_{theor2}$. The image processing analysis suggests that the failure is initiated due to cracking at the wood resin interface propagating parallel to the growth rings. The final drop in axial withdrawal resistance is associated with the crack development and bridging transversely to the growth rings.

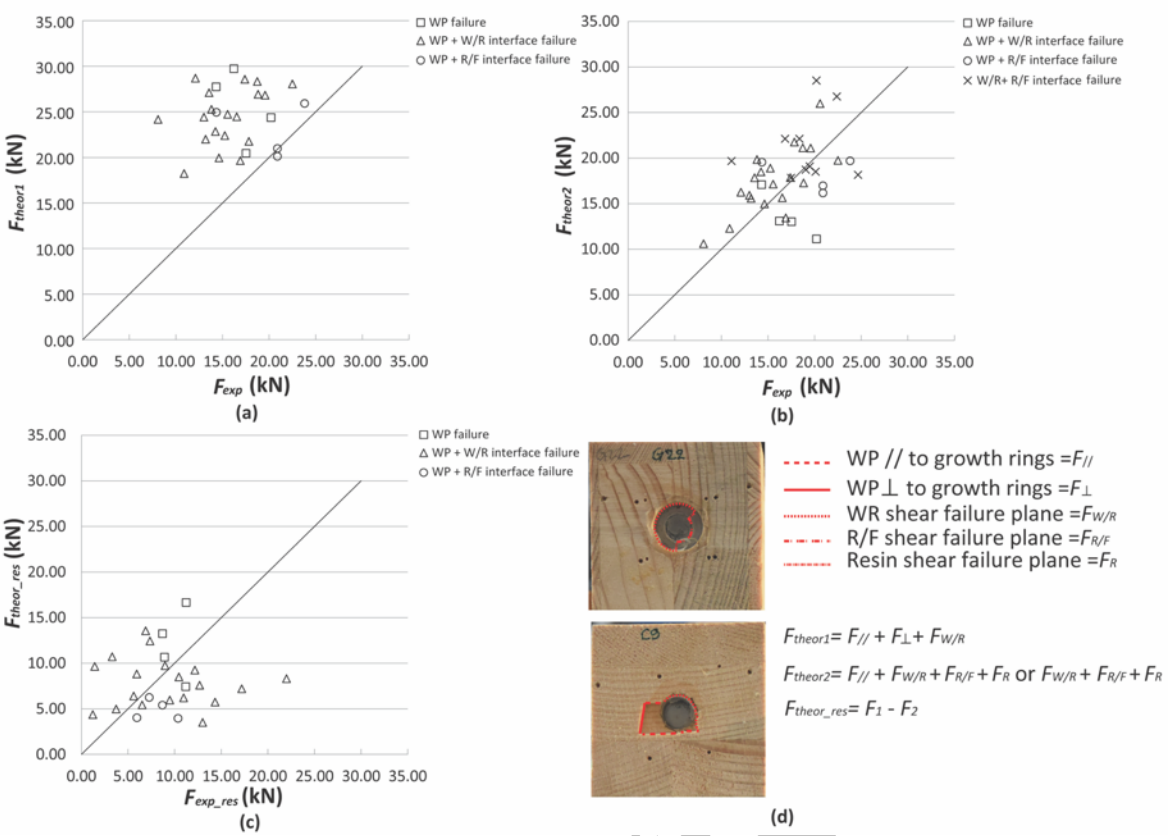

Figure 8: (a) F_{theor1} versus F_{exp}, (b) F_{theor2} versus F_{exp}, (c) F_{theor_res} versus F_{exp_res} and (d) definition of theoretical values according to shear failure planes.

3.6 Material viscous damping ratio

In timber connections with dowels the energy dissipation relies on plastic deformation of timber due to the embedment of the dowel and on the friction losses from the relative slip of the dowel within the timber penetrations. In glued-in rod connections the energy dissipation relies on the creep deformation and hysteresis of the materials (both glue and wood). The material viscous damping of wood ranges between 2.5-10% independent of the wood species [61] and in neat epoxies varies from 0.7 to 0.8% [62]. The chemical composition of the epoxy and the presence or not of nanoparticles (e.g. silica or rubber nanoparticles; [63]) can affect the material viscous damping factor. Under cyclic loading the energy absorption will decrease with increasing load-unload cycles at a given reference load due to viscoelastic creep deformation as depicted in Figure 9. The damping ratios and energy dissipation values, E_p, at each load cycle for every group are summarised in Table 3.

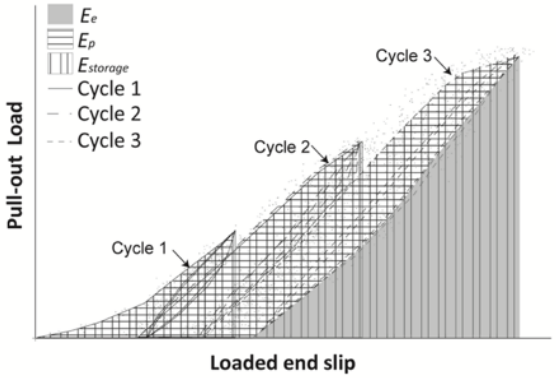

Figure 9: Energy definitions in a load-slip plot under cyclic loading.

In this study the damping ratio is calculated from Equation 1 as defined in [64]

$$\xi = E_p / 2\pi \cdot E_{storage} \quad (1)$$

where $E_{storage}$ is the energy stored during loading and $E_p = E_{storage} - E_e$, where E_p is the energy dissipation and E_e is the elastic energy released during unloading. At each load cycle the final damping ratio was derived as the average value of the damping ratios at each load-unload curve.

Table 3 : Damping ratios

Group	Damping ratio, ξ (%)		
	Cycle 1	Cycle 2	Cycle 3
C-1.5-c	2.3	1.2	0.9
C-3.0-c	3.4	2.5	2.6
C-5.0-c	4.2	3.6	4.2
C-W-c	5.8	9.4	10.1
G-1.5-c	3.2	1.9	3.0
G-3.0-c	3.5	2.7	3.2
G-5.0-c	6.7	8.5	6.8
G-W-c	6.0	8.5	8.1

At each cycle the damping ratio increases with increasing glue-line thickness and the highest values are recorded for the wedge-shaped geometry. This is attributed to the silica nanoparticles that lead to potential microcracking at higher glue-line thicknesses increasing damping and energy dissipation. The glued-in GFRP rods exhibited consistently higher damping ratios compared with the CFRP rods. Despite the increasing trend in the energy dissipation values, E_p, with increasing load, similar trends are not observed in the damping ratio values of the specimens with a constant glue-line thickness. The only exception lies in the wedge-shaped geometry (C-W-c and G-W-C) due to the crack formation and propagation, as discussed in section 3.4, leading to higher energy release and damping. It is expected that the plastic deformation at higher loads in both timber

and glue will lead to higher heat release and energy dissipation due to molecular slippage and failure of intermolecular bonds at microscale. For moment resisting connections with dowels, the equivalent viscous damping has been calculated in the range of 6.24 – 8.19% in the linear elastic range [64] and these values are equivalent to the glued-in FRP rods with the highest glue volume.

3.6 Axial strain distribution

Figures 10a and 10b depict the axial strain distribution along the bonded length for a specimen tested statically with a CFRP and GFRP rod respectively and a glue-line thickness of 5.0 mm. In the plots, x=5.0 mm and x=47.0 mm indicate the loaded and free end respectively, where x is the centre-to-centre distance of the strain gauges along the bonded length.

The axial strain distribution of the CFRP rod specimen is representative of the bond shear stress distribution of a typical adhesive joint where higher shear stresses occur at the ends. Therefore, the axial strain gradient is steeper at the both the free and loaded end and shallower in the remaining bonded length due to the low uniform bond stresses. Deviations are observed for the GFRP rod specimen where an approximately linear strain distribution is observed up to 25% of the failure load, F_u. This indicates uniformly distributed bond stresses.

At higher loads similar strain readings are recorded at the vicinity of the loaded end suggesting that local debonding takes place. At the failure load the maximum strain value is derived at a distance, x=19 mm, followed by a linear strain distribution. The strain reading at x=19 is 4% lower than the theoretical strain value of the GFRP rod due to the applied load. The lower strain value recorded at the loaded end at failure indicates damage of the strain gauge due to the higher slippage at the R/F interface. The GFRP specimen showed a mixed W/R and R/F interface failure. Inspection of the specimens showed unbonded areas and voids as a result of the occupied space from the cables of the strain gauges in combination with the thixotropic nature of the epoxy. The assumption of a uniform bond stress distribution at short bonded lengths to derive the bond stress-slip models in glued-in rod connections [23] deviates at embedment lengths greater than or equal to 5 times the rod diameter due to the local debonding observed.

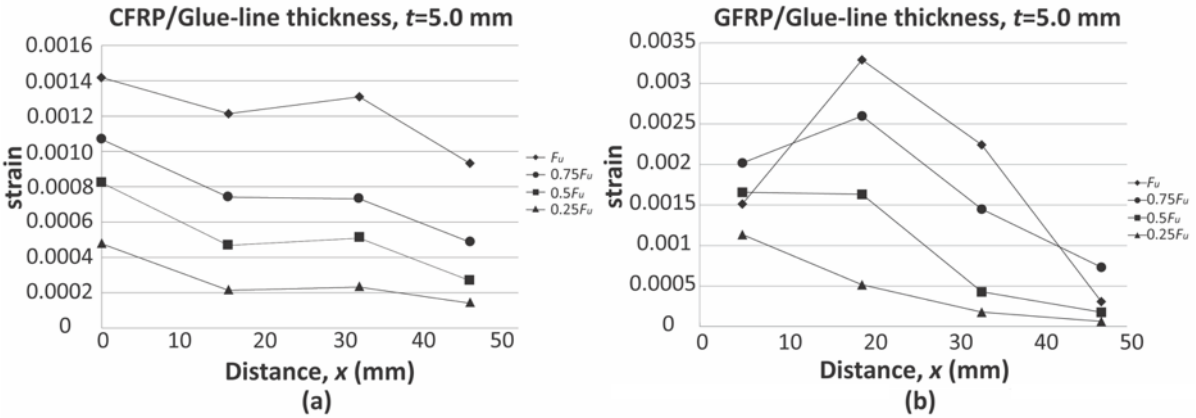

Figure 10: Axial strain distribution for (a) a CFRP rod and (b) for a GFRP rods glued –in timber with a glue-line thickness of t=5.0 mm.

4. Numerical Investigation

4.1 Description of the model

To understand the progressive bond failure mechanism in the wedge shaped geometry, a typical specimen from the G-W-m group was investigated using the FEA package Abaqus/Explicit [65]. To reduce the size of the model and maintain a fine mesh, one quarter of the actual geometry was investigated (see Figure 11). The load was applied in a displacement controlled mode (quasi static analysis). The reaction plate was modelled with rigid elements and the epoxy, GFRP rod and block-laminated timber were modelled with eight-node brick elements with reduced integration (C3D8R). The glue layers between laminations were not considered in timber due to the absence of failures at these interfaces and to decrease computational time. A general contact was applied by assigning local contact properties at the resin/rod and wood/resin interface with hard contact in compression and cohesive behaviour in tension and shear. The contact between the reaction plate and the timber face was modelled using contact interaction with hard contact in compression and friction penalty method in the tangential direction with a 0.3 friction coefficient. A mesh sensitivity analysis was carried out to finalise the degree of discretisation. Distortion control and enhanced hourglass control was applied in the elements of the epoxy. The stiffness of the resin elements was ignored when they exceeded a degradation level of 0.7. Symmetrical boundary conditions were adopted in the X and Y direction.

Both the block-laminated timber and the GFRP rods were modelled as linear elastic orthotropic materials and the mechanical properties are summarised in Table 4. The epoxy was modelled considering a concrete damage plasticity model to simulate the cracking behaviour during pulling out (Table 4). Due to the lack of data from

the manufacturers the engineering constants in Table 4 were derived from the literature for materials that exhibit similar elastic Young's modulus values, E_1.

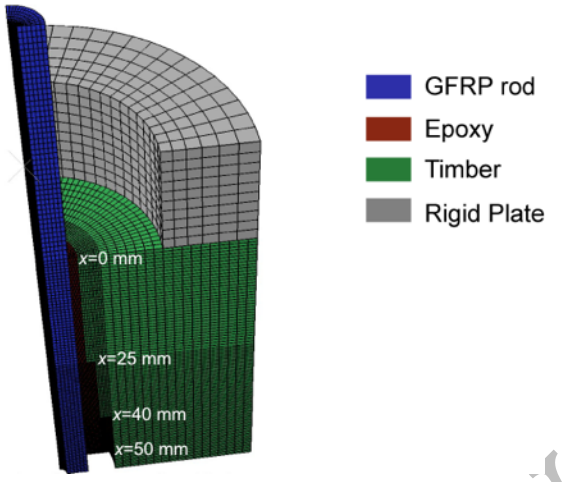

Figure 11: FEA model.

Table 4: Material properties of the FEA model

	E_1 (MPa)	E_2 (MPa)	E_3 (MPa)	ν_{12}	ν_{13}	ν_{23}	G_{12} (MPa)	G_{13} (MPa)	G_{23} (MPa)
Spruce	11600[5]	580[5]	928[5]	0.04[5]	0.04[5]	0.27[5]	880[5]	830[5]	88[5]
GFRP	46000[1]	9100[3]	9100[3]	0.05[3]	0.05[3]	0.25[3]	14000[3]	14000[3]	1300[3]
Epoxy	11200[1]	11200[1]	11200[1]	0.3[1]	0.3[1]	0.3[1]			

Damage Plasticity model									
	Dilation angle	**Eccentri-city**	f_{bo}/f_{co}	K	**Viscocity parameter**	**Compressive behaviour**		**Tensile behaviour**	
						σ_c (MPa)	**Inelastic strain**	σ_t (MPa)	**Fracture Energy (MPa·mm)**
Epoxy	26[4]	0.1 [4]	1.16	1 [4]	0.0001	80[1] 80 8	0 0.083 0.1	24.6[1]	0.43[2]

Note: [1]Nominal values as provided by the manufacturer, [2] Experimentally measured values, [3] Engineering constants from [59], [4] [66], [5]Engineering constants for GL24h from [67].

The strength and stiffness properties of the W/R and R/F interfaces are summarised in Table 5. The shear stiffness values at the W/R interface were derived from linear interpolation of the average experimental stiffness values at SLS from the groups G-1.5-m, G-3.0-m and G-5.0-m and according to the relevant embedment length in the wedge shaped geometry. The tensile normal stiffness of the bond-line was calculated using a ratio of K_{nn}/K_{tt}=2.6 based on data from [68]. The tensile strength of the timber perpendicular to the grain and epoxy were considered at the wood/resin and rod/resin interface accordingly. The shear strength of the bond-lines were

calculated from the average experimental bond strength values of the G-1.5-m, G-3.0-m and G-5.0-m specimens exhibiting clear W/R and R/F interface failure modes.

Table 5: Stiffness and strength properties of the contact zones

Interfacial zone	σ (MPa)	τ_1 (MPa)	τ_2 (MPa)	K_{nn} (MPa/mm)	$K_{tt,1}$ (MPa/mm)	$K_{tt,2}$ (MPa/mm)	δ_f (mm)
W/R	5[1]	5.6[2]	5.6[2]	98.8	38	38	0.2[3]
R/F	24.6[1]	12.7[2]	12.7[2]	156	60	60	0.3[3]

Note: [1]Nominal values as provided by the manufacturer, [2] Experimentally derived values, [3] $\delta_f=\sqrt{\delta_{nn}^2+\delta_{tt,1}^2+\delta_{tt,2}^2}$

4.2 FE Results and Discussion

The pull-out load versus slip results as derived from the FEA model are depicted in Figure 12. The experimental results of the G-W-m group are also presented for ease of comparison. The numerical results agree fairly well with the experiments. A small drop is predicted at a load of 16.7 kN followed by a final failure at 17.5 kN and 0.68 mm loaded end slip. The predicted failure load represents 91% of the average experimental pull-out load. The linear elastic range in the load-deflection plot of the FE model is in accordance with the experimental plots but one specimen, that exhibited the highest stiffness and the highest failure load. Two specimens exhibited lower stiffness at low load levels that can be attributed to any response lag during the test. The equivalent plastic strain, PEEQ, of the epoxy is depicted in Figure 13 at specific load levels representative of progressive resin failure. For ease of comparison an additional view is included where resin elements that have reached resin yielding have been removed (PEEQ>0). The addition of ribs at x=25 and 40 mm causes stress concentrations in the resin during pulling out. Local resin failure at x=25 mm is initiated at low loads of 3.3 kN and cracking propagates up to ultimate tensile failure of the resin at the thinnest glue-line (t=1.5 mm). At approximately 5.0 kN resin yielding is initiated at the tip of the next rib (x=40mm) leading to extended resin yielding at 15.9 kN (Figure 13c). Local resin failure at the loaded end is also observed at the resin/FRP rod interface. At 12.4 kN the highest PEEQ values are observed at the resin/rod interface at x=25 mm and resin failure progressively develops in this interface between x=25 and 50 mm. The local drop in the failure load at 16.7 kN in Figure 12 represents full resin yielding at the resin/rod interface between x=25 and 50 mm at PEEQ=0.20-0.38 (Figure 13d). The numerical results agree well with the experimental bond failure modes where resin/FRP rod failures were detected at the free end, as shown in Figure 7f for a typical G-W-m specimen. In the same specimen through thickness resin failure is also observed both at t=1.5 mm and t=3.0 mm as predicted via the FEA model. The PEEQ values are lower in the thickest rib compared with the thinnest rib and the exact location of resin cracking

can be affected by bridging of microvoids in the resin. At 16.4 kN the PEEQ values decreased towards the free end and resin softening was higher closer to the first rib.

The current model is limited to interfacial bond failure modes and resin failure. The incorporation of the Tsai-Wu failure criterion or Hill's yield criterion in timber and the modelling of the glue layers between laminations can enable prediction of additional failure modes. The dominant bond failure mechanism of the wedge geometry lies at the resin/rod interface and further investigations are needed at longer anchorage lengths for an in-depth understanding of the resin crack development and relationships to progressive bond failure mechanisms. Parametric studies focusing on varying the bonded length of the thinnest glue-line (t=1.5 mm) and the rib geometry (t=3, 5 mm), where different bond failure mechanisms are observed, can take advantage of shear stress concentrations and progressive resin yielding along the bonded length. These can be more informative on progressive bond failure mechanisms and potential pseudo-ductile performance incorporating also a timber failure criterion. The effect of the resin properties on the crack growth and development with the use of a tougher resin is also of interest and subject to further study.

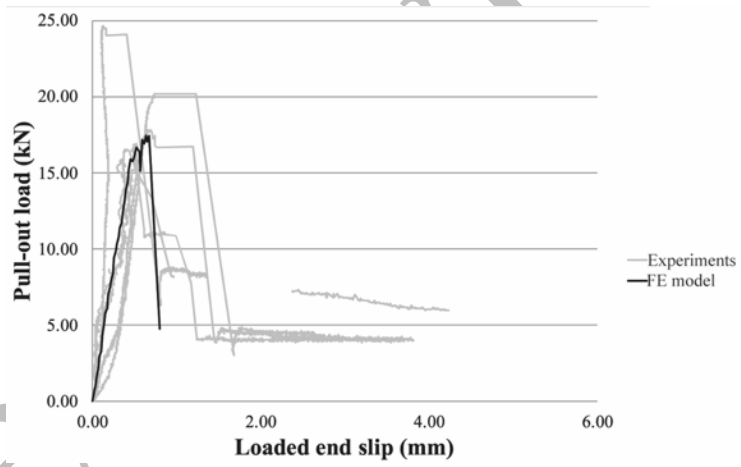

Figure 12: Pull-out load versus loaded end slip for numerical and experimental results

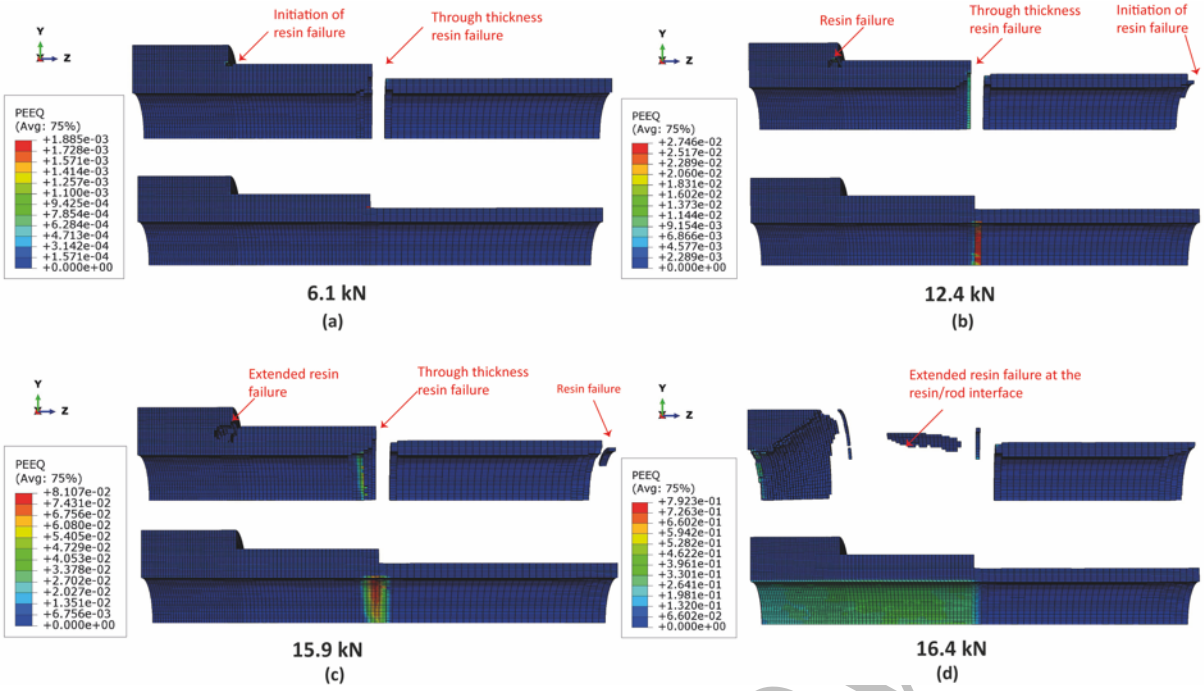

Figure 13: PEEQ values at (a) 6.1 kN, (b) 12.4 kN, (c) 15.9 kN and (d) 16.4 kN.

5 Conclusions

The cyclic loading did not affect the failure load of glued-in FRP rods and leads to higher bond stiffness due to viscoelastic creep deformation. CFRP rods exhibit up to 11% higher bond performance under monotonic loading compared with GFRP rods, but GFRP rods yield higher bond stiffness at SLS, K_{SLS} under the same loading regime. The 'wedge' type and 'inverted wedge' type geometries yield a higher load capacity at a lower glue volume and an increase in the glue-line thickness results in an increase of axial withdrawal capacity. A pseudo-ductile load-deflection response was not observed in the 'wedge' type geometry of the glued-in FRP rods and this was attributed to the short bonded lengths adopted (L=50 mm) An increase in viscous damping was observed with increasing glue volume and 'wedge' type geometries yielded the highest values ξ=5.8-10.1%. The 'inverted wedge' type geometry results in higher bond stiffness due to the presence of a thicker glue-line at the loaded end.

The failure in most specimens is sudden and the failure interface lies at the wood/resin layer. The failure load is related to the shear strength of the interface failure zones as corroborated by the Image processing technique. The 'wedge' type geometry shows a mixed failure mode along the bonded length with a resin/FRP interface failure dominating at the free end. This is verified with an FEA model that shows that resin cracking is initiated at the ribs due to stress concentrations leading to through thickness and resin/FRP interface failure at higher

loads. The FEA model presented here with the use of a CDP model for the resin properties agrees fairly well with the experimental pull-out load versus displacement plots of the G-w-m group. The numerical results combined with the experimental findings can be used in additional parametric studies on progressive bond degradation of glued-in FRP rods at longer anchorage lengths.

Given the considerable difference in cost between the two materials, GFRP rods are the optimum solution for glued-in FRP rod connections in timber. However, the long-term performance of glued-in GFRP and CFRP rods in timber (e.g. under fatigue and sustained loading) should be also investigated in the future to derive firm conclusions. The increase in the glue-line thickness increases significantly the average axial load resistance but this is reflected in a much higher use of glue epoxy and cost.

6 Acknowledgements

The presented work is supported by a Leverhulme Trust Programme Grant "Natural Material Innovation". The timber material was provided by Stora Enso.

7 Data availability statement

The raw/processed data required to reproduce these findings cannot be shared at this time due to technical or time limitations.

8 References

[1] Steiger R, Serrano E, Stepinac M, Rajčić V, O'Neill C, McPolin D, et al. Strengthening of timber structures with glued-in rods. Constr Build Mater. 2015;97:90-105.
[2] Tlustochowicz G, Serrano E, Steiger R. State-of-the-art review on timber connections with glued-in steel rods. Mater Struct. 2011;44(5):997-1020.
[3] EN 1995-1-1: Eurocode 5: Design of timber structures - Part 1-1: General-Common rules and rules for buildings. Bruxelles (Belgium): European Committee for Standardisation CEN; 2004.
[4] DIN EN1995-1-1/NA: 2010-12 (GERMAN NATIONAL ANNEX TO EC5).
[5] New Zealand Design Guide. Timber Industry Federation, NZW14085 SC; 2007.
[6] Madhoushi M, Ansell MP. Experimental study of static and fatigue strengths of pultruded GFRP rods bonded into LVL and glulam. Int J Adhes Adhes. 2004;24(4):319-25.
[7] Zhu H, Faghani P, Tannert T. Experimental investigations on timber joints with single glued-in FRP rods Constr Build Mater. 2017;140:167-72.
[8] Riberholt H. Glued bolts in glulam. Department of Structural Engineering Technical University of Denmark; 1986.
[9] Serrano E. Glued-in rods for timber structures—An experimental study of softening behaviour. Mater. Struct. 2001;34(4):228-34.
[10] Deng JX. Strength of Epoxy Bonded Steel Connections in Glue Laminated Timber. PhD thesis, University of Canterbury; 1997.
[11] Lees JM, Toumpanaki E, Barbezat M, Terrasi GP. Mechanical and Durability Screening Test Methods for Cylindrical CFRP Prestressing Tendons. J Compos Constr. 2017;21(2):04016080.
[12] Feligioni L, Lavisci P, Duchanois G, De Ciechi M, Spinelli P. Influence of glue rheology and joint thickness on the strength of bonded-in rods. Holz als Roh- und Werkstoff. 2003;61(4):281-7.

[13] Ahmad Z, Ansell MP, Smedley D. Epoxy Adhesives Modified With Nano- and Microparticles for In Situ Timber Bonding: FractureToughness Characteristics. J Eng Mater Technol. 2011;133(3):9.
[14] Kinloch AJ, Hunston DL. Effect of volume fraction of dispersed rubbery phase on the toughness of rubber-toughened epoxy polymers. J Mater Sci Lett.1986;5:1207-1209.
[15] Mettem CJ, Bainbridge RJ, Harvey K, Ansell MP, Broughton JG, Hutchinson AR. Evaluation of material combinations for bonded in rods to achieve imporved timber connections. In: Proceedings of the CIB-W18: Meeting 32. Graz, Austria, August, 2000.
[16] Kaufmann M, Kolbe J, Vallée T. Hardwood rods glued into softwood using environmentally sustainable adhesives. J Adhes. 2018;94(11):991-1016.
[17] ACI 440.1R-15 Guide for the Design and Construction of Concrete Reinforced with FRP Bars. Farmington Hills, MI:ACI; 2015.
[18] Goli G, Becherini F, Di Tuccio MC, Bernardi A, Fioravanti M. Thermal expansion of wood at different equilibrium moisture contents. J Wood Sci. 2019;65(1):4.
[19] Raftery GM, Harte AM, Rodd PD. Bonding of FRP materials to wood using thin epoxy gluelines. Int J Adhes Adhes. 2009;29(5):580-588.
[20] Plevris N, Triantafillou TC. Creep Behavior of FRP-Reinforced Wood Members. J Struct Eng. 1995;121(2):174-186.
[21] O'Ceallaigh C, Sikora K, McPolin D, Harte AM. An investigation of the viscoelastic creep behaviour of basalt fibre reinforced timber elements. Constr Build Mater. 2018;187:220-230.
[22] Fava G, Carvelli V, Poggi C. Pull-out strength of glued-in FRP plates bonded in glulam. Constr Build Mater. 2013;43:362-71.
[23] Lorenzis LD, Scialpi V, Tegola AL. Analytical and experimental study on bonded-in CFRP bars in glulam timber. Compos B Eng 2005;36(4):279-89.
[24] Bengtsson C, Johansson CJ. GIROD - Glued in Rods for Timber Structures. 2002. Contract No.: SMT4-CT97-2199.
[25] Plevris N, Triantafillou Thanasis C. FRP-Reinforced Wood as Structural Material. J Mater Civ Eng. 1992;4(3):300-317.
[26] Schober K-U, Harte AM, Kliger R, Jockwer R, Xu Q, Chen J-F. FRP reinforcement of timber structures. Constr Build Mater. 2015;97:106-118.
[27] Sun X, He M, Li Z. Novel engineered wood and bamboo composites for structural applications: State-of-art of manufacturing technology and mechanical performance evaluation. Constr Build Mater. 2020;249:118751.
[28] Raftery GM, Whelan C. Low-grade glued laminated timber beams reinforced using improved arrangements of bonded-in GFRP rods. Constr Build Mater. 2014;52:209-220.
[29] Shekarchi M, Vatani Oskouei A, Raftery GM. Flexural behavior of timber beams strengthened with pultruded glass fiber reinforced polymer profiles. Compos Struct. 2020;241:112062.
[30] Micelli F, Scialpi V, La Tegola A. Flexural Reinforcement of Glulam Timber Beams and Joints with Carbon Fiber-Reinforced Polymer Rods. J Compos Constr. 2005;9(4):337-347.
[31] Nowak TP, Jasieńko J, Czepiżak D. Experimental tests and numerical analysis of historic bent timber elements reinforced with CFRP strips. Constr Build Mater. 2013;40:197-206.
[32] Borri A, Corradi M, Grazini A. A method for flexural reinforcement of old wood beams with CFRP materials. Compos B Eng. 2005;36(2):143-153.
[33] Sena-Cruz J, Branco J, Jorge M, Barros JAO, Silva C, Cunha VMCF. Bond behavior between glulam and GFRP's by pullout tests. Compos B Eng. 2012;43(3):1045-1055.
[34] Blank L. Bending Resistance and Deformation Capacity of Fibre Reinforced Glulam Beams. Zurich: ETH; 2018.
[35] Blank L, Frangi A. Design model for the bending resistance of fibre reinforced glulam. Eng Struct. 2020;211:110385.
[36] Rossignon A, Espion B. Experimental assessment of the pull-out strength of single rods bonded in glulam parallel to the grain. Holz als Roh- und Werkstoff. 2008;66(6):419-432.
[37] Steiger R, Gehri E, Widmann R. Pull-out strength of axially loaded steel rods bonded in glulam parallel to the grain. Mater. Struct. 2007;40(1):69-78.
[38] Meyer N, Blass HJ. Connections with Glued-In Rods In Trusses Made of Beech-LVL. In: Proceedings of the World Conference on Timber Engineering (WCTE 2018): Seoul, Republic of Korea, August, 2018.
[39] Simonin. Goujons collès RESIX. Avis Technique France; 2006. Contract No.: CSTB3/05-453.
[40] Estévez Cimadevila J, Otero Chans D, Martín Gutiérrez E, Vázquez Rodríguez J. New anchoring system with adhesive bulbs for steel rod joints in wood. Constr Build Mater. 2012;30:583-589.
[41] Estévez Cimadevila J, Otero Chans D, Martín Gutiérrez E. Adhesive multi-bulbs: A novel anchoring system using threaded steel rods glued into wood. Constr Build Mater. 2013;48:131-136.
[42] ACI 440.3R-12. Guide Test Methods for Fiber-Reinforced Polymer (FRP) Composites for Reinforcing or Strengthening Concrete and Masonry Structures. Farmington Hills, MI:ACI; 2012.

[43] BS EN ISO 527-1: Plastics. Determination of tensile properties. Brussels: BSI: The British Standards Institution; 2019.
[44] Ayatollahi MR, Shadlou S, Shokrieh MM. Fracture toughness of epoxy/multi-walled carbon nanotube nano-composites under bending and shear loading conditions. Mater Des 2011;32(4):2115-2124.
[45] ASTM D 6980-17: Standard Test Method for Determination of Moisture in Plastics by Loss in Weight. West Conshohocken; 2017.
[46] Faye C, Le Magorou L, Morlier P, Surleau J. French data concerning glued-in rods. In: Proceedings of the CIB-W18: Meeting 37. Edinburgh, UK, August, 2004.
[47] BS EN 301:2017. Adhesives, phenolic and aminoplastic, for load-bearing timber structures. Classification and performance requirements. London, UK: BSI: The British Standards Institution; 2017.
[48] BS EN 338:2016. Structural timber-Strength classes. London, UK: BSI: The British Standards Institution; 2016.
[49] BS 373:1957: Methods of testing small clear specimens of timber. London, UK: BSI: The British Standards Institution; 1957.
[50] ASTM D143 - 14: Standard Test Methods for Small Clear Specimens of Timber. West Conshohocken; 2014.
[51] Broughton JG, Hutchinson AR. Pull-out behaviour of steel rods bonded into timber. Materials and Structures. 2001;34(2):100.
[52] Gehri E. High performing jointing technique using glued-in rods. In: Proceedings of the 11th World Conference on Timber Engineering (WCTE 2010): Riva del Garda, Italy, June, 2010.
[53] Deng JX. Strength of Epoxy Bonded Steel Connections in Glue Laminated Timber, PhD Thesis, University of Canterbury; 1997.
[54] Reynolds T, Sharma B, Harries K, Ramage M. Dowelled structural connections in laminated bamboo and timber. Compos B Eng. 2016;90:232-240.
[55] Tepfers R. Bond of FRP reinforcement in concrete: a state-of-the-art in preparation. Special Publication. 1998;180:493-504.
[56] Aicher S, Wolf M, Gustafsson PJ. Load displacement and bond strength of glued-in rods in timber influenced by adhesive, wood density, rod slenderness and diameter. In: Proceedings of the first RILEM Symposium on Timber Engineering. Stockholm, September, 1999.
[57] De Lorenzis L, Antonio N. Bond between Near-Surface Mounted Fiber-Reinforced Polymer Rods and Concrete in Structural Strengthening. ACI Struct J.99(2).
[58] Achillides Z, Pilakoutas K. Analytical approach to the bond behaviour of FRP bars in concrete. In: Symposium on Bond in Concrete from Research to Standards: Budapest, Hungary, 2002.
[59] Madhoushi M, Ansell MP. Effect of glue-line thickness on pull-out behavior of glued-in GFRP rods in LVL: Finite element analysis. Polym Test. 2017;62:196-202.
[60] Toumpanaki E, Ramage MH. Bond Performance of Glued-in CFRP and GFRP Rods in Timber. In: Proceedings of the International Network of Timber Engineering Research (INTER): Meeting 51. Tallinn, 2018.
[61] Yeh CT, Hartz BJ, Brown CB. Damping sources in wood structures. J.Sound and Vib. 1971;19(4):411-9.
[62] Alva A, Raja S. Damping Characteristics of Epoxy-Reinforced Composite with Multiwall Carbon Nanotubes. Mech Adv Mater Struct. 2014;21(3):197-206.
[63] Huang C-Y, Tsai J-L. Characterizing vibration damping response of composite laminates containing silica nanoparticles and rubber particles. J. Compos Mater. 2014;49(5):545-557.
[64] Loss C, Zonta D, Piazza M. Analytical model to evaluate the equivalent viscous damping of timber structures with dowel-type fastener connections. In: Proceedings of the World Conference on Timber Engineering 2012, WCTE 2012. Auckland, July, 2012. p. 516-525.
[65]ABAQUS,Version2018,documentation,Providence(RI):Dassaultsystemssimuliacrop,2018.
[66] Crocker L, Dean G. Temperature Dependence of the Properties of an Epoxy Adhesive. Middlesex: Materials Centre, National Physical Laboratory; 2001. Contract No.: PAJex1-No 5.
[67] Wood Handbook. Wood as Engineering Material2010.
[68] Azinović B, Danielsson H, Serrano E, Kramar M. Glued-in rods in cross laminated timber – Numerical simulations and parametric studies. Constr Build Mater. 2019;212:431-441.